Received: 12 January 2022 | Revised: 23 March 2022 | Accepted: 24 March 2022

DOI: 10.1002/jcla.24514

RESEARCH ARTICLE

WILEY

RNA demethylase ALKBH5 regulates hypopharyngeal squamous cell carcinoma ferroptosis by posttranscriptionally activating NFE2L2/NRF2 in an m^{6}A-IGF2BP2-dependent manner

Jing Ye[1] | Xiaozhen Chen[2] | Xiaohua Jiang[1] | Zhihuai Dong[1] | Sunhong Hu[1] | Mang Xiao[1]

[1]Department of Otolaryngology Head and Neck Surgery, Sir Run Run Shaw Hospital, College of Medicine, Zhejiang University, Hangzhou, Zhejiang, China

[2]Laboratory of Cancer Biology, Institute of Clinical Science, Sir Run Run Shaw Hospital, College of Medicine, Zhejiang University, Hangzhou, Zhejiang, China

Correspondence
Mang Xiao, Sir Run Shaw Hospital, College of Medicine, Zhejiang University, East Qingchun Road Nr.3, Hangzhou, Zhejiang 310016, China.
Email: joelxm@zju.edu.cn

Funding information
This work was supported by the Natural Science Foundation of Zhejiang Province (no. LY21H160031), the National Natural Science Foundation of China (no. 62071415, 81903160), the Medical Health Science and Technology Project of Zhejiang Provincial Health Commission Grants (no. 2020367813), and Medical Health Science Project of Hangzhou (Grant No. OO20190775, A20210546).

Abstract

Background: Having emerged as the most abundant posttranscriptional internal mRNA modification in eukaryotes, N6-methyladenosine (m^{6}A) has attracted tremendous scientific interest in recent years. However, the functional importance of the m^{6}A methylation machinery in ferroptosis regulation in hypopharyngeal squamous cell carcinoma (HPSCC) remains unclear.

Methods: We herein performed bioinformatic analysis, cell biological analyses, transcriptome-wide m^{6}A sequencing (m^{6}A-seq, MeRIP-seq), RNA sequencing (RNA-seq), and RNA immunoprecipitation sequencing (RIP-seq), followed by m^{6}A dot blot, MeRIP-qPCR, RIP-qPCR, and dual-luciferase reporter assays.

Results: The results revealed that ALKBH5-mediated m^{6}A demethylation led to the posttranscriptional inhibition of NFE2L2/NRF2, which is crucial for the regulation of antioxidant molecules in cells, at two m^{6}A residues in the 3′-UTR. Knocking down ALKBH5 subsequently increased the expression of NFE2L2/NRF2 and increased the resistance of HPSCC cells to ferroptosis. In addition, m^{6}A-mediated NFE2L2/NRF2 stabilization was dependent on the m^{6}A reader IGF2BP2. We suggest that ALKBH5 dysregulates NFE2L2/NRF2 expression in HPSCC through an m^{6}A-IGF2BP2-dependent mechanism.

Conclusion: Together, these results have revealed an association between the ALKBH5-NFE2L2/NRF2 axis and ferroptosis, providing insight into the functional importance of reversible mRNA m^{6}A methylation and its modulators in HPSCC.

KEYWORDS
ALKBH5, ferroptosis, HPSCC, m^{6}A modification, NFE2L2/NRF2

Jing Ye and Xiaozhen Chen authors are contributed equally to this work.

1 | INTRODUCTION

Head and neck squamous cell carcinoma (HNSCC) is considered to be one of the malignancies with the most severe impact on patients' quality of life. HNSCC comprises a heterogeneous group of tumors arising from the mucosal surfaces of the nasal and oral cavities, oropharynx, larynx, and hypopharynx.[1] While hypopharyngeal squamous cell carcinoma (HPSCC) accounts for only 3–4% of HNSCC cases, it is known to be the most invasive type of HNSCC.[2] Although HPSCC treatment has improved considerably, the survival rate of patients with recurrent HPSCC has barely improved due to the lack of effective interventions and precise biomarkers.[3] Therefore, understanding the biological mechanisms of HPSCC malignancy is essential for developing more efficient therapeutic strategies.

The activation of apoptotic cell death is a principal approach to the killing of cancer cells.[4] However, HPSCC cell apoptosis is decreased upon the acquisition of intrinsic resistance to apoptosis.[4] Ferroptosis, is an iron-catalyzed form of regulated necrosis occurring through abundant peroxidation of polyunsaturated fatty acids (PUFAs),[5] is being explored as a possible mechanism for the eradication of apoptosis-resistant cancer cells.[4] Recent studies have shown that erastin and sulfasalazine inhibit head and neck cancer (HNC) cell growth and induce the accumulation of lipid reactive oxygen species (lipid ROS), suggesting that apoptosis-resistant HNSCC cells can be killed via the induction of ferroptosis.[6–8]

Having emerged as the most abundant posttranscriptional internal mRNA modification in eukaryotes, N6-methyladenosine (m^6A) has attracted tremendous scientific interest in recent years. In mammalian cells, m^6A is posttranscriptionally installed by a canonical set of writers, methyltransferase-like 3 (METTL3), methyltransferase-like 14 (METTL14), and Wilms tumor 1-associated protein (WTAP).[7,9] Demethylases, comprising fat-mass and obesity-associated protein (FTO), and AlkB homolog 5 (ALKBH5), can remove m^6A modifications.[10] In addition, m^6A functions via recognizing m^6A reader proteins, and YT521-B homology (YTH) domain-containing family proteins (YTHDF1/2/3) are responsible for mRNA decay.[11] Insulin-like growth factor 2 mRNA-binding proteins (IGF2BP1/2/3) are responsible for stabilizing mRNA. Accumulating evidence has confirmed that multiple biological functions are regulated by m^6A modification. In addition to its contributions to embryonic development disorders, tumorigenesis, homeostasis dysregulation, immune cell differentiation, and nervous system diseases, m^6A modification also facilitates the acquisition of chemoradioresistance, the development of inflammation, and the induction of autophagy in various cancers.[12–14]

Serving as the primary demethylase of m^6A, ALKBH5 plays biological and pharmacological roles in human cancers and noncancer diseases. ALKBH5 plays dual roles in various cancers by regulating diverse biological processes, and the regulatory mechanisms of ALKBH5-dependent m^6A modification are thought to involve long noncoding RNAs (lncRNAs), cancer stem cells, autophagy, and hypoxia.[15] ALKBH5 has also been characterized as a tumor suppressor in various cancers.[16–21] The results of the current study suggest that ALKBH5 directly targets the NFE2L2/NRF2 transcript and mediates its expression in an m^6A-dependent manner. Further study identified NFE2L2/NRF2 as a target of IGF2BP2. Upon ALKBH5 knockdown, NFE2L2/NRF2 transcripts with higher m^6A levels were bound by IGF2BP2, which resulted in enhanced mRNA stabilization and increased protein expression, thus reducing ferroptosis. Together, these findings demonstrated the functional importance of the m^6A methylation machinery in ferroptosis regulation, which expands our understanding of this interplay that is essential for the development of therapeutic strategies in HPSCC.

2 | MATERIALS AND METHODS

2.1 | Patient specimens

Specimens from HPSCC patients at individual medical centers who underwent surgery and regular medical surveillance between 2012 and 2020 were used. All participants provided written informed consent to participate in this study. Paraffin-embedded surgical specimens were stored permanently in the Sir Run Shaw Hospital Pathology Department.

2.2 | Global m^6A measurement

The global m^6A levels in mRNA were measured with an EpiQuik m^6A RNA Methylation Quantification Kit (Colorimetric) (Epigentek, Farmingdale, NY) in accordance with the manufacturer's protocol.

2.3 | m^6A sequencing (m^6A-seq and MeRIP-seq) and RNA sequencing (RNA-seq)

Total RNA was extracted using TRIzol reagent (Invitrogen, CA, USA) following the manufacturer's protocol. The total RNA quality and quantity were analyzed with a Bioanalyzer 2100 and RNA 6000 Nano LabChip Kit (Agilent, CA, USA) and were confirmed to have an RIN > 7.0. Approximately 200 μg of total RNA was used to isolate poly(A) mRNA with poly(T) oligo-coupled magnetic beads (Invitrogen). After purification, the poly(A) mRNA fractions were fragmented into ~100-nt-long oligonucleotide sequences using divalent cations under elevated temperature conditions. Then, the cleaved RNA fragments were incubated for 2 h at 4°C with an m6A-specific antibody (No. 202003, Synaptic Systems, Germany) in IP buffer (50 mM Tris–HCl, 750 mM NaCl and 0.5% Igepal CA-630) supplemented with BSA (0.5 μg/μl). The mixture was then incubated with protein A beads and eluted with elution buffer (1 × IP buffer and 6.7 mM m^6A). The eluted RNA was precipitated with 75% ethanol, and eluted m^6A-containing fragments (IP) and untreated input control fragments were used to construct the final

cDNA library in accordance with a strand-specific library preparation protocol by the dUTP method. The average insert size of the paired-end libraries was ~100 ± 50 bp. Then, we performed paired-end 2 × 150 bp sequencing on an Illumina NovaSeq™ 6000 platform at LC-BIO Biotech Ltd. (Hangzhou, China) in accordance with the vendor's recommended protocol.

2.4 | Anti-m^{6}A immunoprecipitation and RNA immunoprecipitation (RIP)

Cells were washed twice with PBS and collected, and the pellet was then resuspended in IP lysis buffer (150 mM KCl, 25 mM Tris [pH 7.4], 5 mM EDTA, 0.5 mM DTT, 0.5% NP40, 1× protease inhibitor, and 1 U/μl RNase inhibitor). The lysate was harvested by centrifugation at 12,000*g* for 10 min after incubation for 30 min. Antibodies and 40 μl of protein G beads (Invitrogen, USA) were added to the lysate prior to incubation overnight at 4°C. After washing three times with wash buffer (150 mM KCl, 25 mM Tris [pH 7.4], 5 mM EDTA, 0.5 mM DTT, and 0.5% NP40), coprecipitated RNAs were extracted with TRIzol reagent and ethanol-precipitated with glycogen (Invitrogen, USA). The enrichment of RNAs was normalized to that of the IgG immunoprecipitate.

2.5 | Luciferase assay

Fragments of the NRF2-3′-UTR containing the wild-type m^{6}A or mutant m^{6}A motifs (where m6A was replaced by C) were synthesized at Gene Chemistry (Shanghai, China). The firefly luciferase and Renilla luciferase activities in each well were calculated by a dual-luciferase reporter assay system. The ratio of the luciferase activity of the NRF2 3′-UTR reporter to that of the Renilla luciferase control was determined 48 h after siRNA treatment. The relative luciferase activity was further normalized to that in cells transfected with the firefly luciferase vector control and subjected to the same treatment conditions. Firefly luciferase activity and Renilla luciferase activity were measured using a FLUOstar Omega microplate reader (BMG LABTECH, Offenburg, Germany). The results are shown in the form of relative firefly luciferase activity normalized to that of Renilla luciferase. All experiments were repeated three times, and three replicates were conducted for each group.

2.6 | Mouse treatment and tumor biology studies

HPSCC FaDu and Detroit 562 cells (1×10^6) stably expressing the control vector and constructed lentiviral vector were injected subcutaneously into the right flanks of nude mice. The tumor sizes and mouse weights in all groups were measured every 3 days for 1–6 weeks. For NRF2 inhibitor treatment, the right flanks of 4-week-old male nude mice were injected subcutaneously with Detroit 562 and FaDu cells (1×10^6). After 12 days, the mice were divided into the control and NRF2 inhibitor groups ($n = 5$ per group). The NRF2 inhibitor was administered at a concentration of 30 mg/kg by intraperitoneal injection.

All mice were housed in standard cages in a light- and temperature-controlled room and were given standard chow and water. All animal studies were carried out in accordance with the Institute of Laboratory Animal Resources guidelines and were approved by the University Committee on the Use and Care of Animals at Zhejiang University.

2.7 | Statistical analysis methods

Bioinformatic analyses, including GO analysis, KEGG analysis, GSEA, and Circos plot analysis, were performed using the OmicStudio tools at https://www.omicstudio.cn/tool. The analysis of TCGA HNSCC data was performed using GEPIA.[22] NFE2L2/NRF2 functional association data, including protein and gene interaction, pathway, coexpression, and colocalization data, were summarized with GeneMANIA (http://genemania.org). All statistical analyses were carried out using GraphPad Prism version 7 (GraphPad Software, CA) for Windows. Statistical significance was assessed by the unpaired two-tailed Student's *t* test, analysis of variance (ANOVA) or Spearman rank correlation analysis. The data are expressed as the mean ± SD values. $^*p < 0.05$; $^{**}p < 0.01$; $^{***}p < 0.001$. Each experiment was repeated independently at least three times.

More detailed materials and methods are provided in the Supporting information S1.

3 | RESULTS

3.1 | Sensitivity to ferroptosis was associated with the m^{6}A modification level in HNSCC

RSL3 is an activator of ferroptosis and inhibits the activity of GPX4 by covalently bonding with GPX4, which leads to lipid peroxide accumulation.[23] First, we exposed different HNSCC cell lines to RSL3 at various concentrations for 24 h. The Alamar Blue and LDH release assays showed that sensitivity to RSL3 treatment differed considerably between the various HNSCC cell lines. RSL3 reduced the viability (Figure 1A, B) and colony formation ability (Figure S1a) of HPSCC cells (Detroit 562 and FaDu cells), with the sensitivity of OSCC (SCC9 and SCC25) cell lines being substantially reduced. The death of HPSCC cells induced by RSL3 treatment was reversed by cotreatment with the ferroptosis inhibitor liproxstatin-1 (Figure S1b, c).

In addition, RSL3 increased the cellular lipid peroxide (i.e., lipid ROS) levels in HNSCC cell lines to varying degrees. Changes in the cellular lipid ROS levels in these cell lines after RSL3 treatment as determined by BODIPY C11 staining showed similar trends

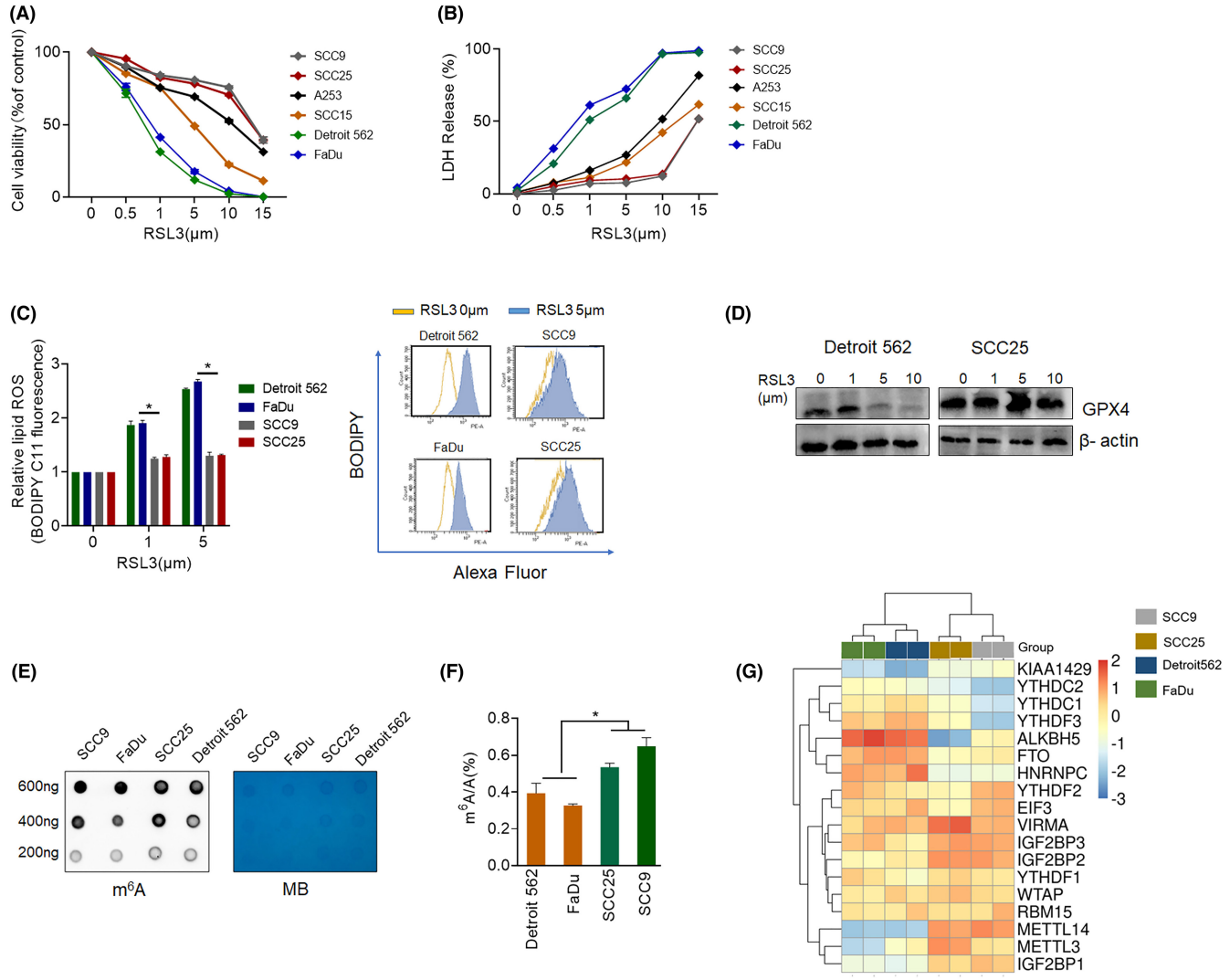

FIGURE 1 RSL3-induced head and neck cancer cell ferroptosis is closely correlated with the global m^{6}A abundance. (A, B) Cell viability (A) and LDH release (B) assays of HNSCC cell lines exposed to different concentrations of RSL3 for 24 h. (C) Measurement of cellular lipid ROS levels by BODIPY C11 staining after exposure to RSL3 for 24 h. (D) Western blot analysis of Detroit 562 and SCC25 cells exposed to various concentrations of RSL3 for 24 h. β-Actin was used as the loading control. (E, F) Representative images of the m^{6}A dot blot assay (E) and quantitation of m^{6}A (F) showing the global m^{6}A abundance in HNSCC cells. MB, methylene blue staining (as a loading control). (G) Heatmap of HNSCC cells with hierarchical clustering of ferroptosis-sensitive and ferroptosis-insensitive cells; each value was normalized to the corresponding mean value

(Figure 1C). RSL3 dose-dependently reduced the protein expression of GPX4 in Detroit 562 HPSCC cells but not in SCC25 cells (Figure 1D).

To explore the correlation between m^{6}A modification and ferroptosis in HNSCC, m^{6}A dot blot and m^{6}A RNA methylation quantification assays were performed. The m^{6}A modification level was significantly decreased in HPSCC cells, which showed increased sensitivity to ferroptosis (Figure 1E, F). Furthermore, qRT–PCR analysis was performed to compare the m^{6}A-regulated gene expression profiles in HPSCC, SCC9, and SCC25 cells. Consistent with the lower m^{6}A modification level in HPSCC cells, the ALKBH5 expression level was significantly higher in HPSCC cells than in the other cell lines (Figure 1G), implying that dysregulation of ALKBH5 may be involved in HPSCC cell ferroptosis.

3.2 | Inhibition of ALKBH5 expression decreased the sensitivity of HPSCC cells to ferroptosis

HPSCC cells were transduced with a lentiviral vector encoding a short hairpin RNA specific for ALKBH5, and the transduction efficiency was validated by qRT–PCR and Western blot (Figure S2a, b). The polyadenylated RNA (poly(A) RNA) m^{6}A level was noticeably increased in shALKBH5 cells compared with wild-type (WT) HPSCC cells, as determined by m^{6}A dot blot (Figure 2A) and EpiQuik™ m6A quantification (Figure S2c) assays.

To determine whether ALKBH5 plays a role in HPSCC cell ferroptosis, Western blotting was performed to compare the expression levels of novel ferroptosis-related genes in shALKBH5 Detroit 562

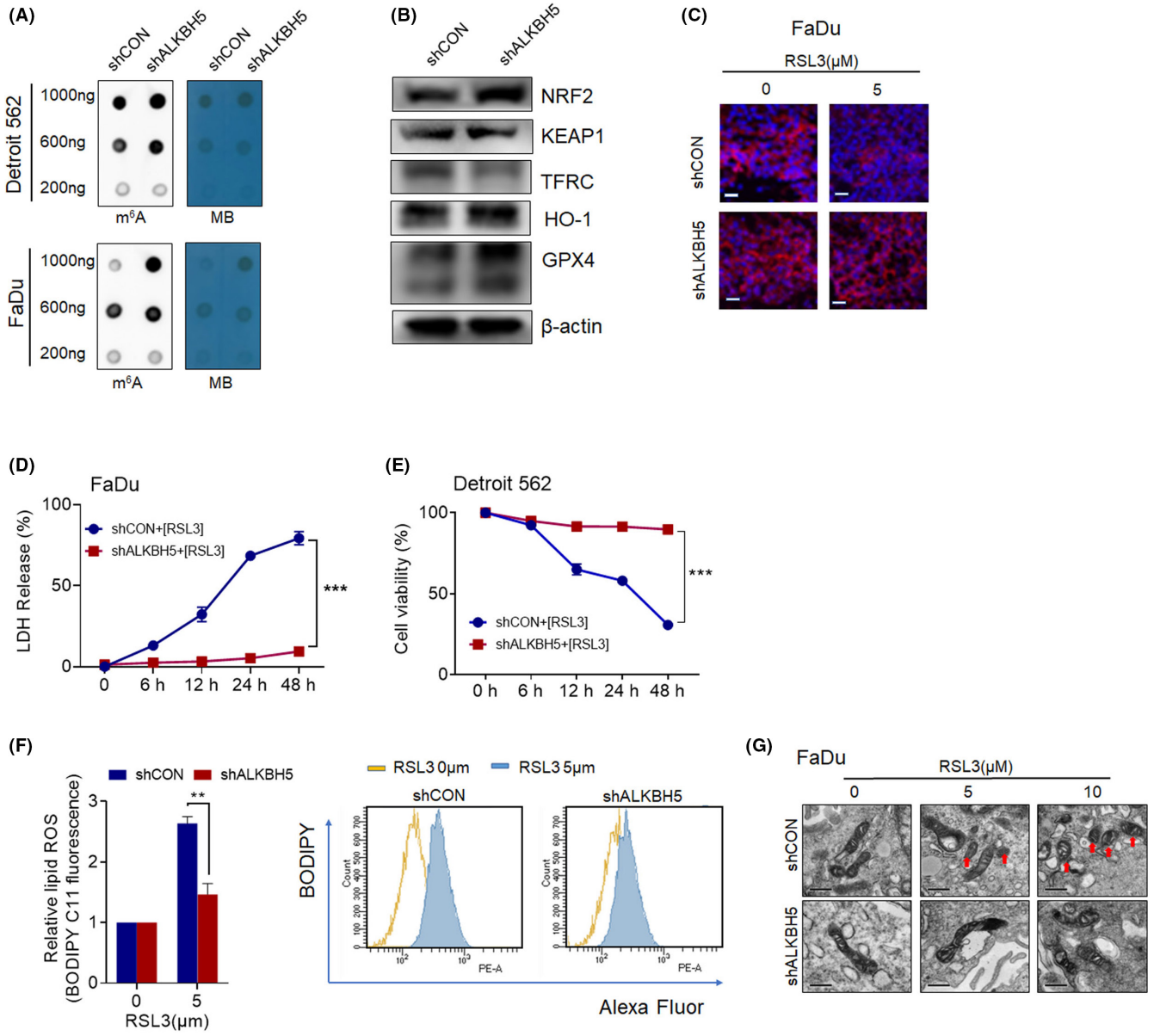

FIGURE 2 ALKBH5 may drive HPSCC cell ferroptosis. (A) m^{6}A dot blot assay of the global m^{6}A abundance in mRNAs of control and shALKBH5HPSCC cells. MB, methylene blue staining (as a loading control). (B) Western blot analysis of the indicated ferroptosis-related proteins in control and shALKBH5 Detroit 562 cells. β-Actin was used as the loading control. (C) Representative immunofluorescence staining of GPX4 (scale bar = 200 μm, magnification: E, 20×) in control and shALKBH5 Detroit 562 cells 24 h after RSL3 treatment. (D) Cell viability assay of control and shALKBH5 Detroit 562 cells 24 h after RSL3 treatment (scale bar = 200 μm, magnification: E, 20×). (E) LDH release assay of control and shALKBH5 Detroit 562 cells 24 h after RSL3 treatment. (F) Measurement of lipid ROS levels in control and shALKBH5 Detroit 562 cells by BODIPY C11 staining after exposure to RSL3 (5 μM) for 24 h. (G) Ultrastructural analysis of shCON and shALKBH5 cells. The red arrows indicate outer membrane rupture (scale bar = 500 nm)

cells and control cells. Knocking down ALKBH5 markedly increased the protein expression levels of GPX4, HO-1, and NRF2 and decreased the protein expression levels of TFRC and Keap1 in shALKBH5 cells but not in control cells (Figure 2B). Immunofluorescence staining showed higher positivity for GPX4 in shALKBH5 cells treated with RSL3 than in control cells (Figure 2C). The inhibition of the ALKBH5 gene significantly reversed RSL3-induced cell death and the increase in the cellular lipid ROS level (Figure 2D-F). In addition, electron microscopy analysis revealed more severe mitochondrial shrinkage in shCON cells than in shALKBH5 FaDu cells treated with RSL3 (Figure 2G). These data suggest that ALKBH5 positively regulates RSL3-induced ferroptosis.

3.3 | Overexpression of ALKBH5 sensitized HPSCC cells to RSL3 in vitro and in vivo

We next examined the effect of ALKBH5 overexpression on the growth and viability of HPSCC cells. The transfection efficiency was validated by qRT–PCR and Western blotting (Figure S2d).

Inhibition of NRF2 and GPX4 was induced by ALKBH5 transfection. Upon overexpression of the ALKBH5 gene by plasmid transfection, the NRF2 and GPX4 expression levels in HPSCC cells were decreased independent of RSL3 treatment (Figure 3A). In addition, ALKBH5 overexpression inhibited the growth and viability of HPSCC cells (Figure 3B-D). Cell death was enhanced by the combination of RSL3 treatment and ALKBH5 plasmid transfection (Figure 3B-D). To clarify the effects of ALKBH5 on HPSCC cells in vivo, ALKBH5-overexpressing and negative control FaDu cells were implanted into BALB/c mice via subcutaneous injection. RSL3

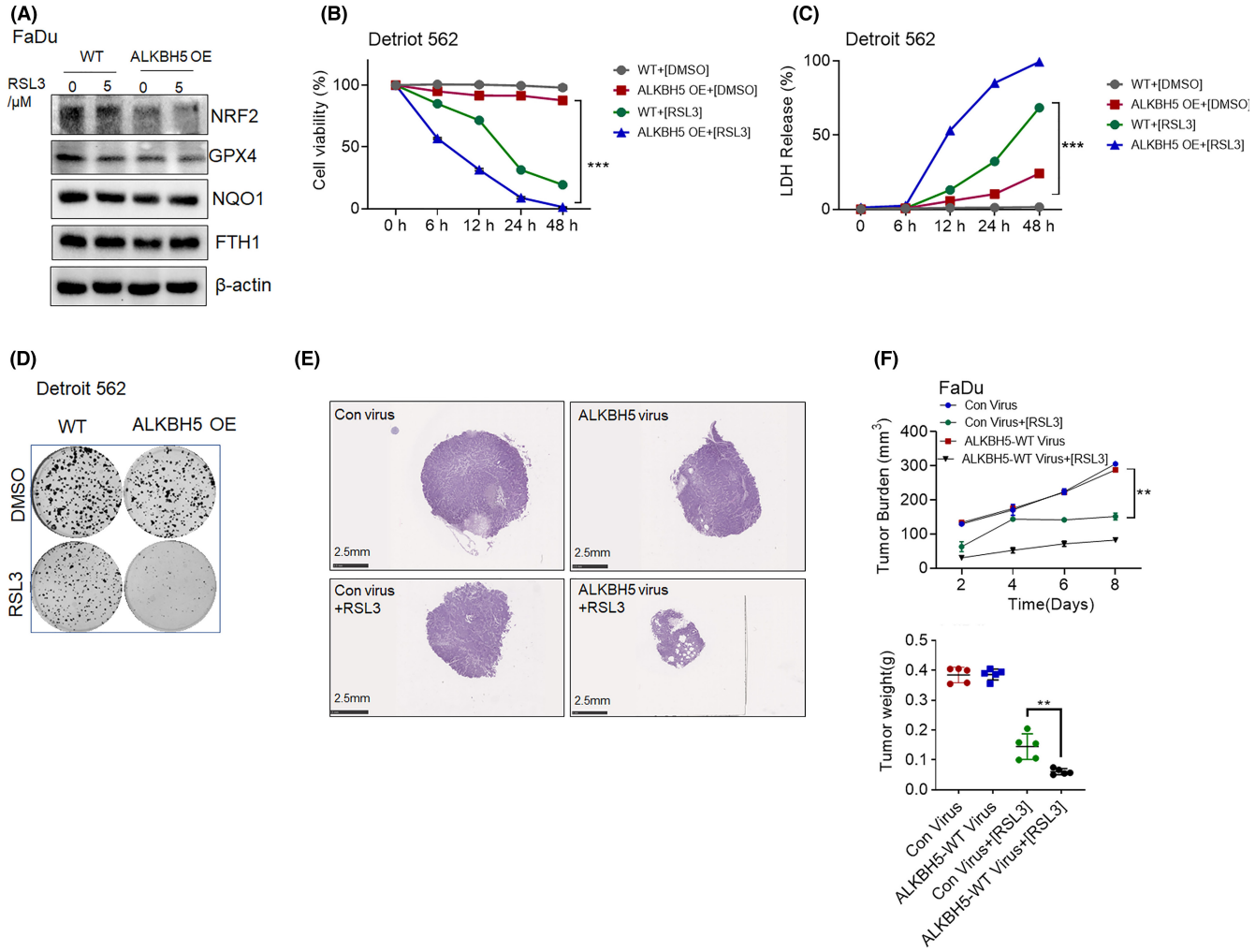

FIGURE 3 Overexpression of ALKBH5 sensitized HPSCC cells to RSL3 in vitro and in vivo. (A, B, C) Cell viability (A), LDH release (B) and colony formation (C) assays were performed on FaDu cells transduced with the control vector or ALKBH5-WT lentiviral vector and subsequently treated with 5 μM RSL3. (D, E, F) Representative images of H&E-stained tissues to evaluate xenograft tumor formation (D), tumor volumes (E), and tumor weights (F) in nude mice bearing tumors comprising Detroit 562 cells transduced with the control vector or ALKBH5-WT lentiviral vector and treated with or without RSL3

FIGURE 4 Transcriptome-wide m^{6}A-seq and RNA-seq analyses identified potential targets of ALKBH5 in HPSCC. (A) m^{6}A motifs in m^{6}A-seq data as detected by the HOMER motif discovery tool. Metagene plot showing nearly unchanged m^{6}A peak distributions and similar GGAC consensus motifs in shCON- and shALKBH5-transfected FaDu cells (both replicates). (B) Density distribution of the m^{6}A peaks across mRNA transcripts. The upstream untranslated region (5′UTR), coding region (CDS), and downstream untranslated region (3′UTR) were divided into 100 segments, and the percentages of peaks within each segment were determined. (C) Proportions of m^{6}A peaks distributed in the 5′UTR, start codon region, CDS, stop codon region and 5′UTR in the entire set of mRNA transcripts. (D) Circos plot showing the distribution of m^{6}A hypermethylation (hyper) and hypomethylation (hypo) peaks in the transcriptomes of human FaDu shALKBH5 cells compared with shCON cells. (E) Distribution of genes with significantly different levels of both m^{6}A ($\log_2$FC) and gene expression ($\log_2$ FC) between shCON and shALKBH5 FaDu cells. (F) Relative RNA levels of the indicated genes in FaDu cells upon ALKBH5 knockdown. (G) Flow chart of the selected candidate ALKBH5 target genes in FaDu cells. (H) IGV tracks displaying the distribution of m^{6}A peaks and ALKBH5 binding peaks across the indicated genes as determined by m^{6}A-seq and RNA-seq analyses of FaDu cells. (I) Sequence analysis of the NFE2L2/NRF2 5′-UTR revealed two matches to the 5′-RRACA-3′ (R = G or A) m^{6}A consensus sequence

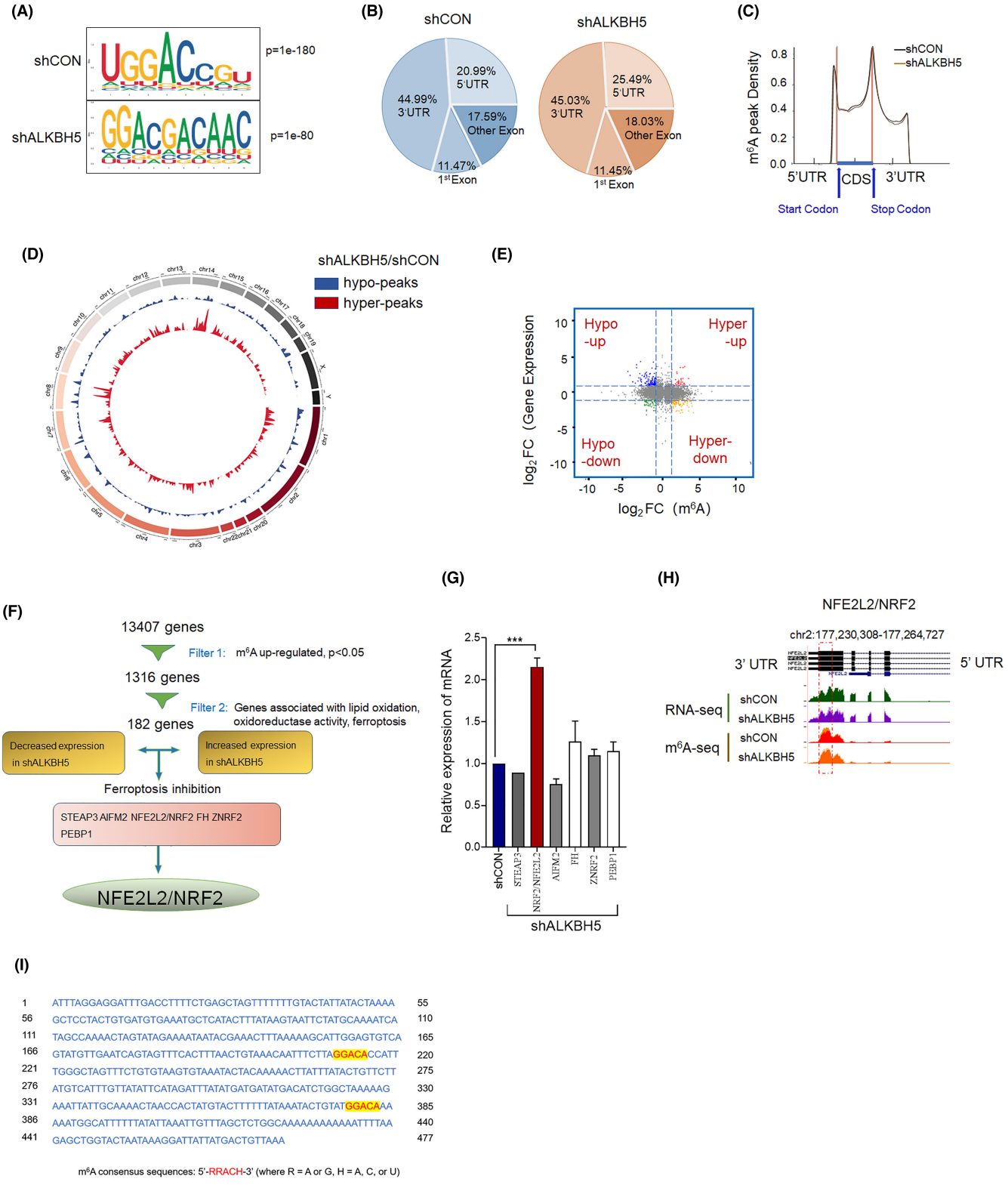

treatment reduced the growth and weights of the xenografted HPSCC tumors in the mice (Figure 3E, F). In addition, overexpression of ALKBH5 significantly enhanced RSL3-induced tumor suppression. These data strongly suggest that ALKBH5 functions as a tumor suppressor gene and mediates HPSCC cell ferroptosis.

3.4 | MeRIP-seq combined with RNA-seq identified potential targets of ALKBH5

To identify potential mRNA targets of ALKBH5 whose m^{6}A levels are decreased by ALKBH5 expression in HPSCC cells, shALKBH5

and control FaDu cells were subjected to transcriptome-wide m^{6}A sequencing (m^{6}A-seq, MeRIP-seq) and RNA sequencing (RNA-seq) analyses. Principal component analysis (PCA) showed that two replicates (shCON: shCON_1 and shCON_2; shALKBH5: shK5_1 and shK5_2) of each sample clustered together, suggesting good repeatability among the two replicates of each group (Figure S3a). Consistent with previous research, the most common m^{6}A motif, "GGAC," was significantly enriched in the m^{6}A peaks (Figure 4A).

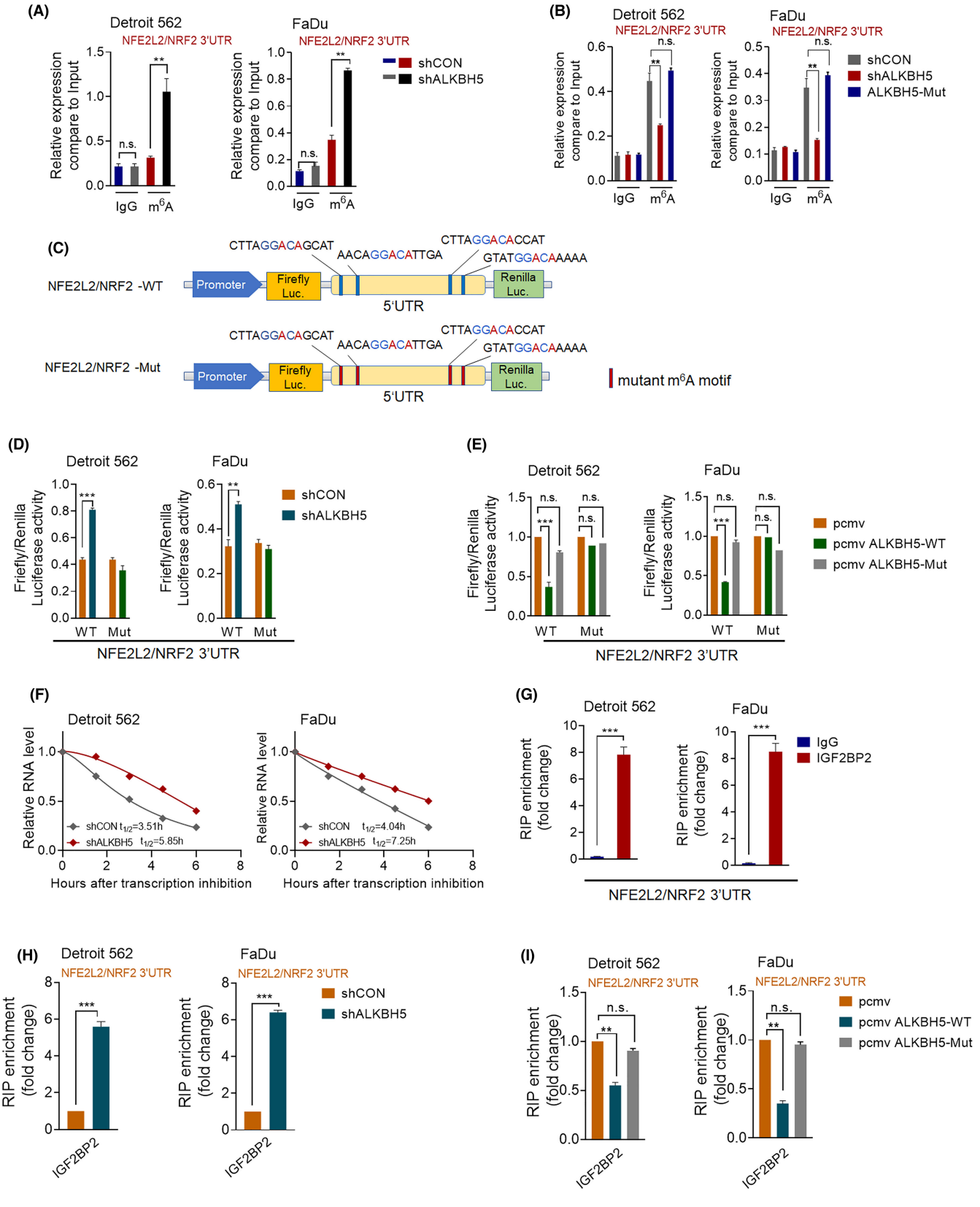

FIGURE 5 ALKBH5 abolishes the mRNA expression and stability of NFE2L2/NRF2 in a manner dependent on its m6A methyltransferase activity. (A) MeRIP-qPCR of the levels of NFE2L2/NRF2 3′UTR m^{6}A modification in control and shALKBH5 Detroit 562 and FaDu cells; $n = 3$, nonparametric Mann–Whitney test. (B) MeRIP-qPCR of the levels of NFE2L2/NRF2 3′UTR m^{6}A modification in GV141, GV141-ALKBH5-Mut (H204A mutant of ALKBH5) and GV141-ALKBH5-WT Detroit 562 and FaDu cells; $n = 3$, nonparametric Mann–Whitney test. (C) Graphical depiction of the protocol used to construct luciferase reporter plasmids expressing the WT or mutant human NFE2L2/NRF2 3′UTR. The relative luciferase activity was calculated as the ratio of firefly luciferase activity to that of Renilla luciferase. (D, E) Luciferase reporter plasmids expressing the WT and mutant human NFE2L2/NRF2 3′UTRs. Luciferase activity was measured in Detroit 562 and FaDu cells transfected with the control (shCON) and shALKBH5 (D) or with GV141, GV141-ALKBH5-Mut (H204A mutant of ALKBH5) and GV141-ALKBH5-WT (E); $n = 3$, nonparametric Mann–Whitney test). (F) The NFE2L2/NRF2 mRNA half-life ($t_{1/2}$) in control and shALKBH5 Detroit 562 and FaDu cells was determined by real-time PCR. The cells were treated with actinomycin D and harvested at the indicated time points. $n = 3$, nonparametric Mann–Whitney test. (G) RIP-qPCR in HPSCC cells showing the direct binding between the IGF2BP2 protein and the NFE2L2/NRF2 3′UTR. (H, I) RIP-qPCR revealed the binding enrichment of IGF2BP2 to the NFE2L2/NRF2 3′UTR in HPSCC cells transfected with the control (shCON) and shALKBH5 (H) or with GV141, GV141-ALKBH5-Mut (H204A mutant of ALKBH5) and pCMV-ALKBH5-WT (I); $n = 3$, nonparametric Mann–Whitney test

RNA-seq revealed 548 downregulated and 564 upregulated transcripts ($p < 0.05$) upon ALKBH5 overexpression (Figure S3b). The peaks were located in protein-coding transcripts and enriched in the 5′UTR and 3′UTR, especially near stop codons, which was consistent with the m^{6}A distribution (Figure 4B, C).

Then, we compared the different mRNA transcripts with altered m^{6}A modifications between control and shALKBH5 cells. m^{6}A-seq analysis revealed overall m^{6}A hypermethylation at the transcript level after the knockdown of ALKBH5 in FaDu cells (Figure 4D). Considering the role of ALKBH5 in the m^{6}A methyltransferase complex, mRNA transcripts with hypermethylated.

m^{6}A peaks in FaDu shALKBH5 cells were identified as possible targets. Based on the RNA-seq data, we identified 967 genes with m^{6}A hypermethylation whose mRNA transcript levels were downregulated ($p < 0.05$, hyper-down) and 49 genes with m^{6}A hypermethylation whose mRNA transcript levels were upregulated ($p < 0.05$, hyper-up) in shALKBH5 cells compared with shCON cells (Figure 4E). GO term and KEGG pathway enrichment analyses revealed that these m^{6}A-hypermethylated gene transcripts ($p < 0.05$) were predominantly enriched in "protein and lipid binding," "lipid metabolic process," "membrane," "endocytosis," and "ferroptosis" (Figure S3c). Additionally, gene set enrichment analysis (GSEA) showed that these genes were enriched in the pathways response to oxidized phospholipids, KEGG oxidative phosphorylation, and missiaglia regulated by methylation up (Figure S3d). This finding is consistent with the observation that the lipid peroxidation of long-chain fatty acids and oxidative phosphorylation are correlated with cell membrane oxidative damage during the ferroptotic process.[24–27] A total of 182 genes involved in ferroptosis, lipid oxidation, and oxidoreductase activity were selected for further validation. Six genes, STEAP3, AIFM2, NFE2L2/NRF2, FH (fumarate hydratase), ZNRF2, and PEBP1, whose alteration suppresses ferroptosis, were finally selected as candidate targets of ALKBH5 (Figure 4F).

Further qRT-PCR analysis showed that the mRNA level of NFE2L2/NRF2 was dramatically increased in shALKBH5FaDu cells (Figure 4G). Integrative Genomics Viewer (IGV) data peak visualization revealed m^{6}A peak enrichment in the 5′UTR of NFE2L2/NRF2 mRNA that was diminished upon ALKBH5 knockdown (Figure 4H, I). Consistent with our results, previously reported m^{6}A, RIP, and CLIP data from the m^{6}A2Target database (http://m6a2target.cancer omics.org/#/search/TFR) identified NFE2L2/NRF2 mRNA as a potential target of ALKBH5 (GSE87515).

NFE2L2/NRF2 plays a crucial role in the regulation of cellular antioxidant molecules. It controls cellular antioxidant systems in cancer cells, playing a key role in protecting against intracellular and environmental stresses.[28,29] NFE2L2/NRF2 is constantly degraded by Keap1 and is activated by the inhibition of Keap1.[30,31] Ferroptosis could be a result of aberrant NRF2 signaling.[32] The inhibition of NFE2L2/NRF2 and the antioxidant response elements (AREs) HO-1, FTH1, and NQO1 in HNC cells has been shown to significantly enhance the antitumor activity of ferroptosis inducers.[33,34] Furthermore, the accumulation of NFE2L2/NRF2-ARE proteins during ferroptosis was found to reduce the sensitivity of HNC cells to the GPX4 inhibitors RSL3 and ML-162.[35] Taken together, these findings indicate that NFE2L2/NRF2 may be the direct target of ALKBH5.

3.5 | ALKBH5 decreases the mRNA expression and stability of NFE2L2/NRF2 in a manner dependent on its m^{6}A methyltransferase activity

MeRIP-qPCR assays targeting potential m^{6}A sites were then performed to confirm ALKBH5-dependent m^{6}A demethylation of the 3′UTR of NFE2L2/NRF2 mRNA. Compared with that in the IgG group (pulldown control), the 3′UTR of NFE2L2/NRF2 mRNA was enriched by immunoprecipitation with an m^{6}A-specific antibody (Figure 5A). Western blotting and qRT–PCR were then performed to confirm that NFE2L2/NRF2 expression was upregulated in shALKBH5FaDu cells (Figure S4a).

To determine whether the demethylase activity of ALKBH5 decreases NFE2L2/NRF2 expression, recombinant ALKBH5 mutant (ALKBH5-Mut, NM_017758, H204A) plasmids were constructed. Then, the level of NFE2L2/NRF2 m^{6}A modification was measured after the transfection of control, ALKBH5-WT and ALKBH5-Mut plasmids. The MeRIP-qPCR data showed that overexpression of ALKBH5-WT but not ALKBH5-Mut led to a dramatic decrease in the level of NFE2L2/NRF2 m^{6}A modification in Detroit 562 cells (Figure 5B). In addition, overexpression of ALKBH5 but not ALKBH5-Mut dramatically decreased NFE2L2/NRF2 expression (Figure S4b).

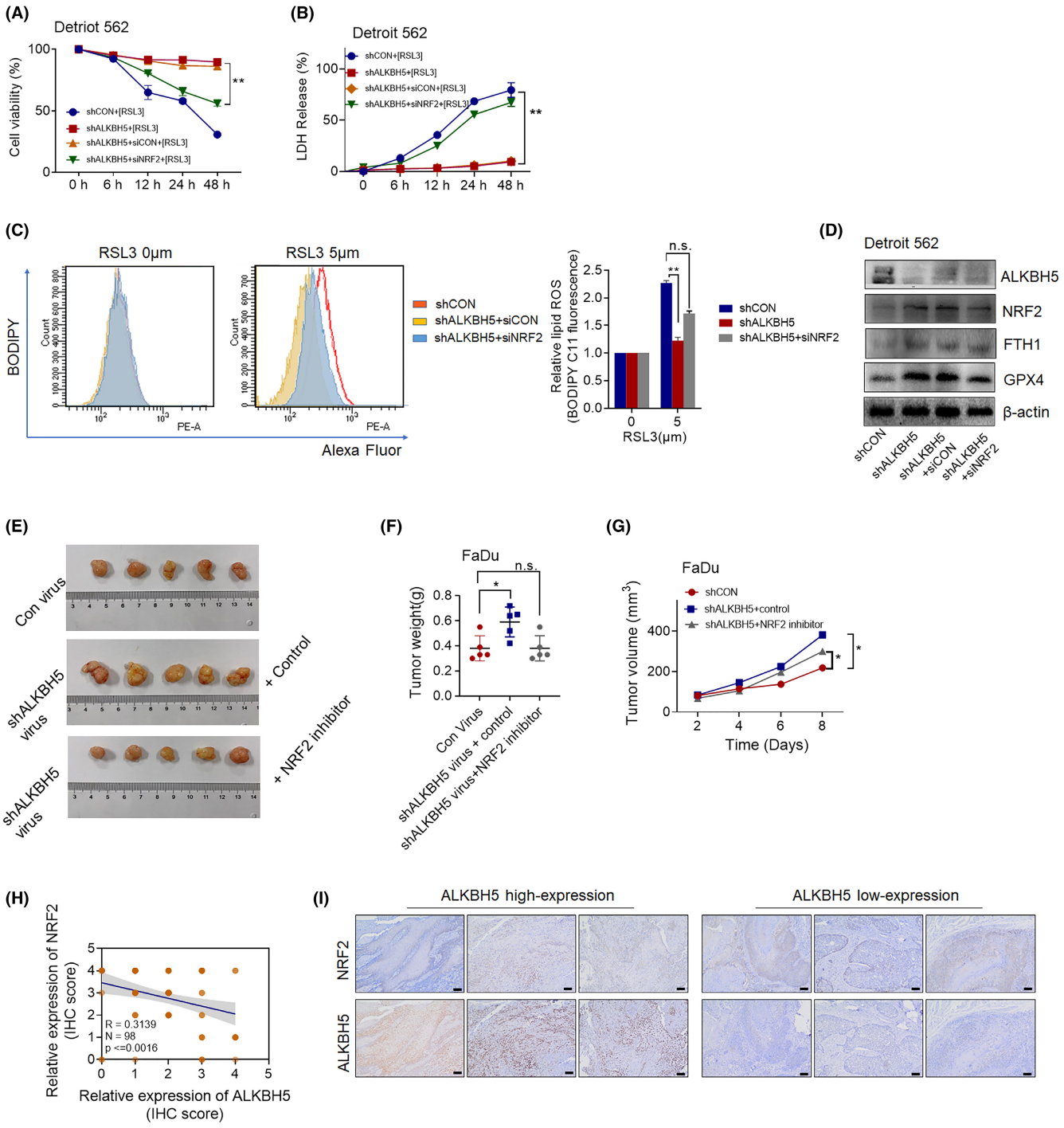

FIGURE 6 NFE2L2/NRF2 is a functionally essential target gene of ALKBH5 in HPSCC. (A, B) Cell viability (A) and LDH release (B) assays were performed with control and shALKBH5 Detroit 562 cells transfected with the control vector (siCON) or NFE2L2/NRF2 siRNA (siNRF2) and subsequently treated with 5 μM RSL3. (C) Western blot analysis of the NFE2L2/NRF2, GPX4, and FTH1 levels after silencing NFE2L2/NRF2 (siNRF2) in Detroit 562 control and shALKBH5 cells. (D) Lipid ROS levels in control and shALKBH5 Detroit 562 cells after transfection with siCON or siNRF2 and exposure to RSL3 (5 μM) for 24 h as determined by BODIPY C11 staining. (E, F, G) Representative images of H&E-stained tissues to evaluate the xenograft tumor formation (E), tumor weights (F) and tumor volumes (G) in nude mice bearing tumors comprising FaDu cells transfected with the control vector or shALKBH5 lentiviral vector and treated with or without ML385 (30 mg/kg, intraperitoneal injection). (H) Pearson rank correlation analysis of the ALKBH5 and NFE2L2/NRF2 protein levels in HPSCC patient tissues as determined by IHC. (I) Representative IHC images of ALKBH5 and NFE2L2/NRF2 in HPSCC patient tissues. Scale bar = 100 μm (40×)

Thereafter, to assess the effect of m^{6}A modification on NFE2L2/NRF2 gene expression, we constructed both wild-type and mutant NFE2L2/NRF2 luciferase reporter plasmids, in which N^6-methylated adenosine (A) residues were replaced with C (cytosine) residues in NFE2L2/NRF2 mRNA with intact m^{6}A sites (Figure 4I, Figure 5C, Figure S4c). As expected, compared with

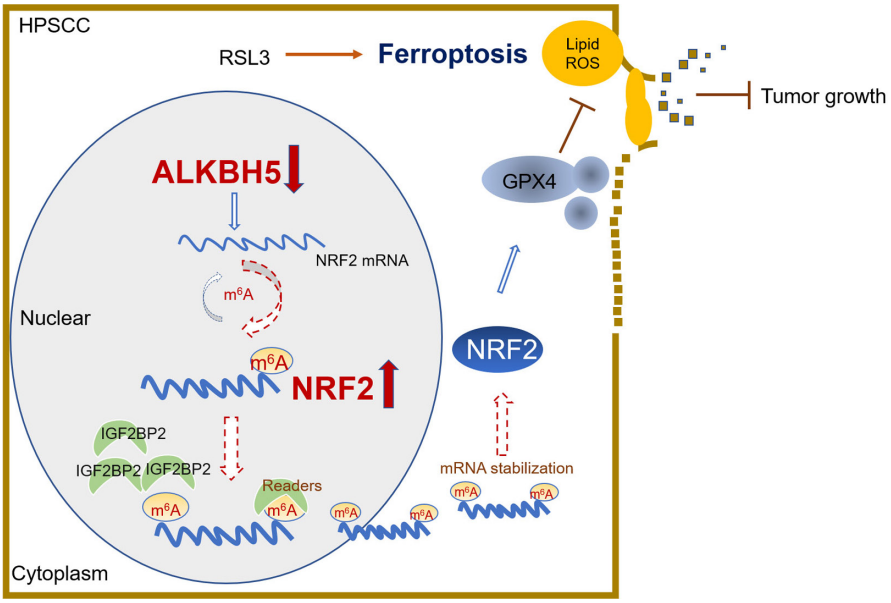

FIGURE 7 Schematic illustration proposed to summarize the relationship among ALKBH5, m^{6}A modification, cell death, and ferroptosis

shCON, shALKBH5 substantially increased the luciferase activity of the individual reporter (firefly/Renilla) constructs containing the wild-type NFE2L2/NRF2 3′UTR. However, ALKBH5 knockdown had no such significant effect on the NFE2L2/NRF2-Mut luciferase reporter activity in Detroit 562 and FaDu cells (Figure 5D). Furthermore, overexpression of ALKBH5 but not the ALKBH5 mutant significantly reduced the luciferase activity of individual reporter (firefly/Renilla) constructs containing the wild-type NFE2L2/NRF2 3′UTR (Figure 5E). Overexpression of ALKBH5 and ALKBH5-Mut had no such significant effect on the NFE2L2/NRF2 3′UTR luciferase reporter activity (Figure 5E).

The m^{6}A modification is interpreted by its readers, such as YTH domain-containing proteins, to regulate mRNA fate and by insulin-like growth factor 2 mRNA-binding proteins (IGF2BPs; including IGF2BP1/2/3) to promote the stability and storage of their target mRNAs in an m^{6}A-dependent manner under both physiological and stress conditions and therefore affects gene expression output.[36] To analyze the effect of m^{6}A modification on the stability of ALKBH5 target transcripts, we conducted RNA stability assays. The RNA stability curves showed that knockdown of ALKBH5 prolonged the half-life of NFE2L2/NRF2 mRNA in HPSCC cells (Figure 5F). qRT–PCR data showed that the knockdown of IGF2BP2, rather than IGF2BP1/3, significantly reduced the mRNA level of NFE2L2/NRF2 in HPSCC cells (Figure S4d, e). Furthermore, the half-life of NFE2L2/NRF2 mRNA was significantly shortened upon the suppression of IGF2BP1 expression (Figure S4f). Notably, the NFE2L2/NRF2 expression level was positively correlated with the IGF2BP2 level in the TCGA HNSCC dataset (Figure S4g).[22] The RIP assay results suggested that IGF2BP2 bound to the 3′UTR of NFE2L2/NRF2 mRNA (Figure 5G), and RIP-PCR indicated that knockdown of ALKBH5 significantly enhanced the binding efficiency of IGF2BP2 to the 3′UTR of NFE2L2/NRF2 mRNA (Figure 5H). In addition, overexpression of ALKBH5-WT but not ALKBH5-Mut significantly abolished the binding efficiency of IGF2BP2 to the 3′UTR of NFE2L2/NRF2 mRNA (Figure 5I).

3.6 | NFE2L2/NRF2 is a functionally essential target gene of ALKBH5 in HPSCC

We next performed rescue experiments to determine whether NFE2L2/NRF2 contributes to the biological function of ALKBH5 in HPSCC. Control and shALKBH5 Detroit 562 cells were transfected with control and siNFE2L2/NRF2 (siNRF2) plasmids, while control and shALKBH5FaDu cells were transfected with control and NFE2L2/NRF2-WT plasmids. The transfection efficiencies were confirmed by qRT–PCR and Western blot analysis (Figure S5a, b). NFE2L2/NRF2 overexpression downregulated the protein expression of GPX4 and FTH1 in shALKBH5 cells (Figure S5c). Cell viability, LDH release, and colony formation assays showed that silencing NFE2L2/NRF2 impaired the growth and viability of shALKBH5 cells (Figure 6A-C). Silencing NFE2L2/NRF2 also significantly increased the lipid ROS levels in shALKBH5 cells (Figure 6D). NFE2L2/NRF2 overexpression also led to significant restoration of the growth and viability of ALKBH5-overexpressing cells (Figure S5d, e). These results suggest that NFE2L2/NRF2 is a critical target gene of ALKBH5 in HPSCC cells. Inhibition of GPX4 renders HNC cells susceptible to ferroptosis, while activation of the NRF2–ARE system induces resistance to GPX4 inhibition.[23,35] Both the light chain and heavy chain of ferritin (FTL and FTH1, respectively), which store iron, as well as ferroportin (SLC40A1), which is responsible for cellular iron efflux, are controlled by NRF2.[37,38] Furthermore, Western blot analysis showed that silencing NFE2L2/NRF2 restored the protein levels of GPX4 and FTH1 in shALKBH5 cells (Figure 6E). Analysis of TCGA HNSCC datasets also revealed that the GPX4 level was positively correlated with the NFE2L2/NRF2 expression level (Figure S5f).[22]

Thus, these results indicated that ALKBH5 may function as a tumor suppressor by abolishing the mRNA stability and expression of NFE2L2/NRF2 in HPSCC cells, thereby promoting their ferroptosis. Several small-molecule NRF2 inhibitors have been developed as antitumor drug candidates.[39,40] We treated mice bearing shALKBH5 and control xenograft tumors with one NRF2 inhibitor, ML385.[41,42] ML385 efficiently inhibited the growth and weights of tumors comprised of shALKBH5 cells in nude mice (Figure 6F-H). We next performed immunohistochemistry (IHC) analyses of HPSCC and paracancerous tissues from patients to further explore the correlation between the expression levels of ALKBH5 and NFE2L2/NRF2 in HPSCC tissues. As expected, ALKBH5 expression was inversely correlated with NFE2L2/NRF2 expression (Figure 6I,J). Taken together, these data show that NFE2L2/NRF2 mediates the regulatory effect of ALKBH5 on HPSCC cell ferroptosis.

4 | DISCUSSION

m^6A modification employs direct control over RNA metabolic processes, including mRNA processing, mRNA export, translation initiation, mRNA stability, and lncRNA biogenesis and thus influences various aspects of cell function.[43] m^6A modulates gene expression, thereby regulating cellular processes ranging from differentiation and apoptosis to therapeutic resistance and immune responses.[44,45]

ALKBH5-dependent m^6A demethylation is involved in the splicing and production of mRNAs with longer 3′-UTRs. The regulatory mechanisms of ALKBH5-dependent m^6A modification are thought to involve lncRNAs, cancer stem cells, autophagy, and hypoxia. In epithelial ovarian cancer (EOC), ALKBH5 upregulation impairs autophagy and facilitates cell proliferation and invasion.[46] METTL3 alleviates autophagic flux in hypoxia/reoxygenation-treated cardiomyocytes, and ALKBH5 can reverse this effect.[16] Our results herein first revealed a critical association between ALKBH5-NFE2L2/NRF2 and ferroptosis in HPSCC (Figure 7). Knockdown of ALKBH5 dramatically suppressed the cellular response to RSL3-induced ferroptosis, and overexpression of ALKBH5 markedly enhanced ferroptotic cell death and lipid peroxidation.

Ferroptosis is an iron-dependent, lipid peroxidation-driven cell death program that shows great potential for cancer therapy.[38,47] Several small molecules have been identified to mediate ferroptosis initiation and ferroptosis sensitivity in different cancers.[38,47] Clearly understanding the sensitivity of cancer cells to ferroptosis is beneficial for the clinical application of drugs targeting ferroptosis in cancer therapy. Notably, we found that ALKBH5 expression enhanced the sensitivity of HPSCC cells to ferroptosis in an m^6A-dependent manner.

NFE2L2/NRF2 was determined to be a downstream target of ALKBH5-mediated m^6A modification by RNA-seq and m^6A-seq analyses, and this relationship that was further confirmed by MeRIP-qPCR analysis, luciferase assays and qRT–PCR assays in control and shALKBH5FaDu cells. Many studies have highlighted that NFE2L2/NRF2 is a critical mitigator of both lipid peroxidation and ferroptosis, established NRF2 target genes that mitigate these pathways, and identified the relevance of the NRF2-lipid peroxidation-ferroptosis axis in disease.[38] The Keap1-NRF2 antioxidant system is involved in RSL3-induced resistance,[48,49] and the NFE2L2/NRF2-induced inhibition or p62 silencing was found to sensitize chemoresistant HNC cells to RSL3. The activation of the NRF2-ARE pathway was found to contribute to the resistance of HNC cells to GPX4 inhibition, and inhibition of this pathway reversed the ferroptotic resistance of HNC cells. As discussed in detail in prior studies, GPX4 is an established NFE2L2/NRF2 transcript target and an integral protein that reduces lipid peroxide levels via an antiferroptotic mechanism.[32,38,50] NFE2L2/NRF2 functional association data, including protein and gene interaction, pathway, coexpression, and colocalization data, were summarized with GeneMANIA (http://genemania.org). Therefore, we did not herein explore the potential mechanisms by which NFE2L2/NRF2 regulates GPX4-dependent lipid peroxidation in detail.

An essential link exists between NFE2L2/NRF2 function and iron homeostasis,[38] and we previously revealed that YTHDF1 is closely correlated with iron metabolism and tumor progression in HPSCC. Mechanistically, YTHDF1 enhances transferrin receptor (TFRC) expression through an m^6A-dependent mechanism.[51] To determine whether YTHDF1 recognizes m^6A modifications on NFE2L2/NRF2, we reanalyzed the sequencing data for YTHDF1-knockdown and control FaDu cells. The m^6A-seq data indicated m^6A peaks associated with mRNA and gene expression changes. However, this finding could not be validated by MeRIP-qPCR (data not shown). Thus, we speculated that ALKBH5 stabilizes NFE2L2/NRF2 through RNA stabilization, as the defined m^6A site is located near the m^6A-enriched regions in the 5′ UTR. We then observed significantly augmented NFE2L2/NRF2 mRNA stability in HPSCC cells upon IGF2BP2 knockdown. The RIP assay confirmed the binding between IGF2BP2 and NFE2L2/NRF2 mRNA. Additionally, functional rescue experiments were performed, and silencing NFE2L2/NRF2 impaired the growth and increased the lipid ROS levels of shALKBH5 cells (Figure 6A-D).

In addition, the NRF2 inhibitor had an anticancer effect on shALKBH5 xenograft tumors (Figure 6F-H). As ALKBH5 functions as a tumor suppressor by inducing the ferroptosis of HPSCC cells, we speculated that targeting NRF2 may be more efficient in tumors with low ALKBH5 expression due to the inhibition of ferroptosis resistance. These hypotheses need to be validated in vivo in the future.

The prognostic value and role of ALKBH5 in HPSCC progression may not have been fully revealed in the present study. Indeed, the role of ALKBH5 in human cancers remains controversial. ALKBH5 has been found to play both oncogenic and tumor-suppressive roles in various cancers.[15] In our study, ALKBH5 was characterized as a critical regulator linking ferroptosis and m^6A modification. Therefore, ALKBH5 could mediate ferroptosis sensitivity in HPSCC. The therapeutic efficacy of ferroptosis induction is higher

for HPSCC tumors with high ALKBH5 expression than for those with low ALKBH5 expression.

Taken together, our findings indicate that ALKBH5 leads to impaired mRNA stability and decreased expression of NFE2L2/NRF2 in HPSCC cells through an m^{6}A-IGF2BP2-dependent mechanism. Our study has uncovered a critical association between ALKBH5-NFE2L2/NRF2 and ferroptosis, providing insight into the functional importance of reversible mRNA m^{6}A methylation and its modulators in HPSCC.

AUTHOR CONTRIBUTIONS

Mang Xiao contributed to conceptulization, data curation, funding acquisition, supervision, validation, and writing—review and editing. Jing Ye and Xiaozhen Chen contributed to methodology and project administration. Jing Ye, Bing Liao, Xiaozhen Chen contributed to formal analysis. Xiaohua Jiang contributed to investigation. Sunhong Hu contributed to resources. Zhihuai Dong contributed to software. Jing Ye contributed to visualization. Jing Ye and Mang Xiao contributed to roles/Writing—original draft.

CONFLICT OF INTEREST

The authors have no competing interests to declare.

DATA AVAILABILITY STATEMENT

Original RNA-seq, overlapping m6A-seq, and RNA-seq data as well as the original patient data from the Sir Run Run Shaw Hospital Biological Specimen Bank are accessible for noncommercial purposes upon request.

PATIENT CONSENT

The protocol was approved by the Ethical Review Committee of Sir Run Run Shaw Hospital, College of Medicine, Zhejiang University. Patient tissue samples were obtained with informed consent. The in vivo assay of nude mice was approved by the Ethics Review Committee of Zhejiang University College of Medicine.

PERMISSION TO REPRODUCE MATERIAL FROM OTHER SOURCES

Not applicable.

CLINICAL TRIAL REGISTRATION

Not applicable.

ORCID

Mang Xiao https://orcid.org/0000-0002-7131-6251

REFERENCES

1. Peltanova B, Raudenska M, Masarik M. Effect of tumor microenvironment on pathogenesis of the head and neck squamous cell carcinoma: a systematic review. *Mol Cancer*. 2019;18(1):63.
2. Yamashita Y, Ikegami T, Suzuki M, et al. Hypopharyngeal cancer risk in Japanese: genetic polymorphisms related to the metabolism of alcohol- and tobacco-associated carcinogens. *J Cancer Res Ther*. 2019;15(3):556-563.
3. Joo YH, Lee YS, Cho KJ, et al. Characteristics and prognostic implications of high-risk HPV-associated hypopharyngeal cancers. *Plos One*. 2013;8(11):e78718.
4. Hassannia B, Vandenabeele P, Vanden BT. Targeting ferroptosis to iron out cancer. *Cancer Cell*. 2019;35(6):830-849.
5. Dixon SJ, Lemberg KM, Lamprecht MR, et al. Ferroptosis: an iron-dependent form of nonapoptotic cell death. *Cell*. 2012;149(5):1060-1072.
6. Liu K, Hu H, Jiang H, et al. Upregulation of secreted phosphoprotein 1 affects malignant progression, prognosis, and resistance to cetuximab via the KRAS/MEK pathway in head and neck cancer. *Mol Carcinog*. 2020;59(10):1147-1158.
7. Roh JL, Kim EH, Jang HJ, Park JY, Shin D. Induction of ferroptotic cell death for overcoming cisplatin resistance of head and neck cancer. *Cancer Lett*. 2016;381(1):96-103.
8. Zhao M, Mydlarz WK, Zhou S, Califano J. Head and neck cancer cell lines are resistant to mitochondrial-depolarization-induced apoptosis. *ORL J Otorhinolaryngol Relat Spec*. 2008;70(4):257-263.
9. Meyer KD, Jaffrey SR. Rethinking m^{6}A readers, writers, and erasers. *Annu Rev Cell Dev Bi*. 2017;33(1):319-342.
10. Nettersheim D, Berger D, Jostes S, Kristiansen G, Lochnit G, Schorle H. N6-Methyladenosine detected in RNA of testicular germ cell tumors is controlled by METTL3, ALKBH5, YTHDC1/F1/F2, and HNRNPC as writers, erasers, and readers. *Andrology-Us*. 2019;7:498-506.
11. Wang X, Lu Z, Gomez A, et al. N6-methyladenosine-dependent regulation of messenger RNA stability. *Nature*. 2014;505(7481):117-120.
12. Shriwas O, Mohapatra P, Mohanty S, Dash R. The impact of m^{6}A RNA modification in therapy resistance of cancer: implication in chemotherapy, radiotherapy, and immunotherapy. *Front Oncol*. 2020;10:612337.
13. Wang X, Wu R, Liu Y, et al. M(6)a mRNA methylation controls autophagy and adipogenesis by targeting Atg5 and Atg7. *Autophagy*. 2020;16(7):1221-1235.
14. Liu S, Li G, Li Q, et al. The roles and mechanisms of YTH domain-containing proteins in cancer development and progression. *Am J Cancer Res*. 2020;10(4):1068-1084.
15. Wang J, Wang J, Gu Q, et al. The biological function of m^{6}A demethylase ALKBH5 and its role in human disease. *Cancer Cell Int*. 2020;20:347.
16. Song H, Feng X, Zhang H, et al. METTL3 and ALKBH5 oppositely regulate m(6)a modification of TFEB mRNA, which dictates the fate of hypoxia/reoxygenation-treated cardiomyocytes. *Autophagy*. 2019;15(8):1419-1437.
17. Tang B, Yang Y, Kang M, et al. M(6)a demethylase ALKBH5 inhibits pancreatic cancer tumorigenesis by decreasing WIF-1 RNA methylation and mediating Wnt signaling. *Mol Cancer*. 2020;19(1):3.
18. Zhang C, Samanta D, Lu H, et al. Hypoxia induces the breast cancer stem cell phenotype by HIF-dependent and ALKBH5-mediated m^{6}A-demethylation of NANOG mRNA. *Proc Natl Acad Sci*. 2016;113(14):E2047-E2056.
19. Shriwas O, Priyadarshini M, Samal SK, et al. DDX3 modulates cisplatin resistance in OSCC through ALKBH5-mediated m(6)A-demethylation of FOXM1 and NANOG. *Apoptosis*. 2020;25:233-246.
20. Zhang J, Guo S, Piao HY, et al. ALKBH5 promotes invasion and metastasis of gastric cancer by decreasing methylation of the lncRNA NEAT1. *J Physiol Biochem*. 2019;75(3):379-389.
21. Yang P, Wang Q, Liu A, Zhu J, Feng J. ALKBH5 holds prognostic values and inhibits the metastasis of colon cancer. *Pathol Oncol Res*. 2020;26(3):1615-1623.
22. Tang Z, Li C, Kang B, Gao G, Li C, Zhang Z. GEPIA: a web server for cancer and normal gene expression profiling and interactive analyses. *Nucleic Acids Res*. 2017;45(W1):W98-W102.
23. Yang WS, Sriramaratnam R, Welsch ME, et al. Regulation of ferroptotic cancer cell death by GPX4. *Cell*. 2014;156(1–2):317-331.

24. Cao JY, Dixon SJ. Mechanisms of ferroptosis. *Cell Mol Life Sci*. 2016;73(11–12):2195-2209.
25. Imai H, Matsuoka M, Kumagai T, Sakamoto T, Koumura T. Lipid peroxidation-dependent cell death regulated by GPx4 and ferroptosis. *Curr Top Microbiol Immunol*. 2017;403:143-170.
26. Latunde-Dada GO. Ferroptosis: role of lipid peroxidation, iron and ferritinophagy. *Biochim Biophys Acta*. 2017;1861(8):1893-1900.
27. Xie Y, Hou W, Song X, et al. Ferroptosis: process and function. *Cell Death Differ*. 2016;23(3):369-379.
28. Gorrini C, Harris IS, Mak TW. Modulation of oxidative stress as an anticancer strategy. *Nat Rev Drug Discov*. 2013;12(12):931-947.
29. Kumari S, Badana AK, Murali Mohan G, Shailender G, RamaRao M. Reactive oxygen species: a key constituent in cancer survival. *Biomark Insights*. 2018;13:91914689.
30. Madden SK, Itzhaki LS. Structural and mechanistic insights into the Keap1-Nrf2 system as a route to drug discovery. *Biochim Biophys Acta Proteins Proteom*. 2020;1868(7):140405.
31. Turpaev KT. Keap1-Nrf2 signaling pathway: mechanisms of regulation and role in protection of cells against toxicity caused by xenobiotics and electrophiles. *Biochemistry (Mosc)*. 2013;78(2):111-126.
32. Salazar M, Rojo AI, Velasco D, de Sagarra RM, Cuadrado A. Glycogen synthase kinase-3beta inhibits the xenobiotic and antioxidant cell response by direct phosphorylation and nuclear exclusion of the transcription factor Nrf2. *J Biol Chem*. 2006;281(21):14841-14851.
33. Kim EH, Jang H, Shin D, Baek SH, Roh JL. Targeting Nrf2 with wogonin overcomes cisplatin resistance in head and neck cancer. *Apoptosis*. 2016;21(11):1265-1278.
34. Roh JL, Kim EH, Jang H, Shin D. Nrf2 inhibition reverses the resistance of cisplatin-resistant head and neck cancer cells to artesunate-induced ferroptosis. *Redox Biol*. 2017;11:254-262.
35. Shin D, Kim EH, Lee J, Roh JL. Nrf2 inhibition reverses resistance to GPX4 inhibitor-induced ferroptosis in head and neck cancer. *Free Radic Biol Med*. 2018;129:454-462.
36. Huang H, Weng H, Sun W, et al. Recognition of RNA N(6)-methyladenosine by IGF2BP proteins enhances mRNA stability and translation. *Nat Cell Biol*. 2018;20(3):285-295.
37. Saito H. Metabolism of iron stores. *Nagoya J Med Sci*. 2014;76(3–4):235-254.
38. Dodson M, Castro-Portuguez R, Zhang DD. NRF2 plays a critical role in mitigating lipid peroxidation and ferroptosis. *Redox Biol*. 2019;23:101107.
39. Lin H, Qiao Y, Yang H, et al. Small molecular Nrf2 inhibitors as chemosensitizers for cancer therapy. *Future Med Chem*. 2020;12(3):243-267.
40. Panieri E, Saso L. Potential applications of NRF2 inhibitors in cancer therapy. *Oxid Med Cell Longev*. 2019;2019:8592348.
41. Tang Z, Zhao L, Yang Z, et al. Mechanisms of oxidative stress, apoptosis, and autophagy involved in graphene oxide nanomaterial anti-osteosarcoma effect. *Int J Nanomed*. 2018;13:2907-2919.
42. Singh A, Venkannagari S, Oh KH, et al. Small molecule inhibitor of NRF2 selectively intervenes therapeutic resistance in KEAP1-deficient NSCLC tumors. *ACS Chem Biol*. 2016;11(11):3214-3225.
43. Chang G, Leu JS, Ma L, Xie K, Huang S. Methylation of RNA N(6)-methyladenosine in modulation of cytokine responses and tumorigenesis. *Cytokine*. 2019;118:35-41.
44. He L, Li H, Wu A, Peng Y, Shu G, Yin G. Functions of N6-methyladenosine and its role in cancer. *Mol Cancer*. 2019;18(1):176.
45. Panneerdoss S, Eedunuri VK, Yadav P, et al. Cross-talk among writers, readers, and erasers of m(6)a regulates cancer growth and progression. *Sci Adv*. 2018;4(10):r8263.
46. Zhu H, Gan X, Jiang X, Diao S, Wu H, Hu J. ALKBH5 inhibited autophagy of epithelial ovarian cancer through miR-7 and BCL-2. *J Exp Clin Cancer Res*. 2019;38(1):163.
47. Xu T, Ding W, Ji X, et al. Molecular mechanisms of ferroptosis and its role in cancer therapy. *J Cell Mol Med*. 2019;23(8):4900-4912.
48. Fan Z, Wirth AK, Chen D, et al. Nrf2-Keap1 pathway promotes cell proliferation and diminishes ferroptosis. *Oncogenesis*. 2017;6(8):e371.
49. Agyeman AS, Chaerkady R, Shaw PG, et al. Transcriptomic and proteomic profiling of KEAP1 disrupted and sulforaphane-treated human breast epithelial cells reveals common expression profiles. *Breast Cancer Res Treat*. 2012;132(1):175-187.
50. Osburn WO, Wakabayashi N, Misra V, et al. Nrf2 regulates an adaptive response protecting against oxidative damage following diquat-mediated formation of superoxide anion. *Arch Biochem Biophys*. 2006;454(1):7-15.
51. Ye J, Wang Z, Chen X, et al. YTHDF1-enhanced iron metabolism depends on TFRC m(6)a methylation. *Theranostics*. 2020;10(26):12072-12089.

SUPPORTING INFORMATION

Additional supporting information may be found in the online version of the article at the publisher's website.

How to cite this article: Ye J, Chen X, Jiang X, Dong Z, Hu S, Xiao M. RNA demethylase ALKBH5 regulates hypopharyngeal squamous cell carcinoma ferroptosis by posttranscriptionally activating NFE2L2/NRF2 in an m^6A-IGF2BP2-dependent manner. *J Clin Lab Anal*. 2022;36:e24514. doi: 10.1002/jcla.24514